NUMERICAL STUDY OF A FLEXIBLE SAIL PLAN: EFFECT OF PITCHING DECOMPOSITION AND ADJUSTMENTS

B. Augier, Naval academy Research Institute, France, benoit.augier@ecole-navale.fr
F. Hauville, Naval academy Research Institute, France, frederic.hauville@ecole-navale.fr
P. Bot, Naval academy Research Institute, France, patrick.bot@ecole-navale.fr
J. Deparday, Naval academy Research Institute, France, julien.deparday@ecole-navale.fr
M. Durand, K-EPSILON company, France, mathieu@k-epsilon.com

Abstract

A numerical investigation of the dynamic Fluid Structure Interaction (FSI) of a yacht sail plan submitted to harmonic pitching is presented to analyse the effects of motion simplifications and rigging adjustments on aerodynamic forces. It is shown that the dynamic behaviour of a sail plan subject to yacht motion clearly deviates from the quasi-steady theory. The aerodynamic forces presented as a function of the instantaneous apparent wind angle show hysteresis loops. These hysteresis phenomena do not result from a simple phase shift between forces and motion. Plotting the hysteresis loops in the appropriate coordinate system enables the associated energy to be determined. This amount of exchanged energy is shown to increase almost linearly with the pitching reduced frequency and to increase almost quadratically with the pitching amplitude in the investigated ranges. The effect of reducing the real pitching motion to a simpler surge motion is investigated. Results show significant discrepancies on the aerodynamic forces amplitude and the hysteresis phenomenon between pitching and surge motion. However, the superposition assumption consisting in a decomposition of the surge into two translations normal and collinear to the apparent wind is verified. Then, simulations with different dock tunes and backstay loads highlight the importance of rig adjustments on the aerodynamic forces and the dynamic behaviour of a sail plan.

NOMENCLATURE

A	deg	pitching oscillation amplitude
C	m	sail plan chord at z_a (from head-sail leading edge to mainsail trailing edge)
C_x		driving force coefficient
$\bar{C_x}$		mean value of C_x
C_y		heeling force coefficient
dx		displacement along x axis at z_a
f_r		flow reduced frequency
S	m^2	total sail area
T	s	pitching oscillation period
V_{AW}	$m.s^{-1}$	apparent wind speed
V_{TW}	$m.s^{-1}$	true wind speed
V_r		flow reduced velocity
W		work associated to hysteresis loop area
z_a	m	height of the centre of aero. forces
β_{AW}	deg	apparent wind angle
β_{eff}	deg	effective wind angle
β_{TW}	deg	true wind angle
ϕ	deg	heel angle
θ	deg	trim angle
α	deg	heading angle
ρ	$kg.m^{-3}$	fluid density
τ	s	phase shift

1 INTRODUCTION

When analysing the behaviour of yacht sails, an important difficulty comes from the Fluid Structure Interaction (FSI) of the air flow and the sails and rig [19, 14, 9]. Yacht sails are soft structures whose shapes change according to the aerodynamic loading. The resulting modified shape affects the air flow and thus, the aerodynamic loading applied to the structure. This Fluid Structure Interaction is strong and non-linear, because sails are soft and light membranes which experience large displacements and accelerations, even for small stresses. As a consequence, the actual sail's shape while sailing — the so-called flying shape — is different from the design shape defined by the sail maker and is generally not known. Recently, several authors have focused on the Fluid Structure Interaction (FSI) problem to address the issue of the impact of the structural deformation on the flow and hence the aerodynamic forces generated [5, 22].

Another challenging task in modelling racing yachts is to consider the yacht behaviour in a realistic environment [6, 19, 14, 9]. Traditional Velocity Prediction Programs (VPPs) used by yacht designers consider a static equilibrium between hydrodynamic and aerodynamic forces. Hence, the force models classically used are estimated in a steady state. However, in realistic sailing conditions, the flow around the sails is most often largely unsteady because of wind variations, actions of the crew and more importantly because of yacht motion due to waves. To account for this dynamic behaviour, several Dynamic Velocity Prediction Programs (DVPPs) have been developed, e.g. by Masuyama et al.[21, 20], Richardt et al. [23], Keuning et al.[18] which need models of dynamic aerodynamic and hydrodynamic forces. While the dynamic effects on hydrodynamic forces have been largely studied, the unsteady aerodynamic behaviour of the sails has received much less attention. Shoop et al.[26] first developed an unsteady aeroelastic model in potential flow dedicated to flexible mem-

branes but neglected the inertia. In a quasi-static approach, a first step is to add the velocity induced by the yacht's motion to the steady apparent wind to build an instantaneous apparent wind (see [23, 18]) and to consider the aerodynamic forces corresponding to this instantaneous apparent wind using force models obtained in the steady state. In a recent study, Gerhardt et al. [15] developed an analytical model to predict the unsteady aerodynamics of interacting yacht sails in 2D potential flow and performed 2D wind tunnel oscillation tests with a motion range typical of a 90-foot (26m) racing yacht (International America's Cup Class 33). Recently, Fossati et al. [10, 11, 12] studied the aerodynamics of model-scale rigid sails in a wind tunnel, and showed that a pitching motion has a strong and non-trivial effect on aerodynamic forces. They showed that the relationship between instantaneous forces and apparent wind deviates — phase shifts, hysteresis — from the equivalent relationship obtained in a steady state, which one could have thought to apply in a quasi-static approach. They also investigated soft sails in the same conditions to highlight the effects of the structural deformation [13].

In a previous work [4], the aero-elastic behaviour of the sail plan subjected to a simple harmonic pitching was numerically investigated. This study has shown hysteresis phenomena between the aerodynamic forces and instantaneous apparent wind angle, which were more pronounced in the FSI case on a realistic soft structure than on a rigid structure. However, in this first work [4], the question of genuine hysteresis phenomenon versus simple phase shift between both oscillating signals was not clearly elucidated. Moreover, the energy associated to the hysteresis phenomenon was not determined. Hence, the first aim of the present work is to investigate further this hysteresis phenomenon to elucidate the hysteresis versus phase shift issue and to determine the associated energy.

Most of studies about the unsteady effect due to yacht pitching have considered a 2D simplified problem and thus approximated the pitching motion by a translational oscillation aligned with the yacht centreline [7, 15]. Then, the usual procedure is to decompose this motion in oscillations perpendicular to and along the direction of the incident flow, which result in oscillations of apparent wind angle and speed respectively (Fig.7). The second aim of this work is to investigate the effects of such simplifications in the yacht motion considered by comparing the results obtained with the sail plan subjected to different types of motion.

The third aim of this work is to address the effect of various rig and sail trims and adjustments on the unsteady aeroelastic behaviour of the sail plan subjected to pitching. This is investigated by comparisons of results obtained for realistic docktunes and backstay tensions used while racing a 28-foot (8m, J80 class) cruiser-racer.

An unsteady FSI model has been developed and validated with experiments in real sailing conditions [1, 2, 3]. Calculations are made on a J80 class yacht numerical model with her standard rigging and sails designed by the sail maker DeltaVoiles. The FSI model is briefly presented in section 2. The methodology of the dynamic investigation is given in section 3. In the continuity of a previous work [4], section 4 gives further precisions on the dynamic behaviour.

The analysis of pitching motion decomposition in simple translation is given in section 5 and the effects of various dock tunes and backstay loads are presented in sections 6.1 and 6.2. In the last section, some conclusions of this study are given, with ideas for future work.

2 NUMERICAL MODEL

To numerically investigate aero-elastic problems which can be found with sails, the company K-Epsilon and the Naval Academy Research Institute have developed the unsteady fluid-structure model ARAVANTI made by coupling the inviscid flow solver AVANTI with the structural solver ARA. The ARAVANTI code is able to model a complete sail boat rig in order to predict forces, tensile and shape of sails according to the loading in dynamic conditions. For more details, the reader is referred to [25] for the fluid solver AVANTI and to [16] and [24] for the structural solver ARA and the FSI coupling method.

ARAVANTI model has been validated. Numerical and experimental comparisons with the model ARAVANTI are based on measurements at full scale on an instrumented 28-foot yacht (J80 class, 8m). The time-resolved sails' flying shape, loads in the rig, yacht's motion and apparent wind have been measured in both sailing conditions of flat sea and moderate head waves and compared to the simulation. The code has shown its ability to simulate the rig's response to yacht motion forcing, and to correctly estimate the loads. Thereby, ARAVANTI is a reliable tool to study the dynamic behaviour of a sail plan subject to pitching motion. For a detailed description of the experimental system and the numerical and experimental comparison, see [1, 2, 3].

3 SIMULATION PROCEDURE

The yacht motion in waves induces unsteady effects in the sails' aerodynamics. In this paper we will study separately one degree of freedom, by applying simple harmonic pitching. The reference frame and the coordinate system attached to the yacht are illustrated in Figure 1.

3.1 Reference steady case

First, the reference steady case is computed with the following parameters: true wind speed at 10m height V_{TW}=6.7 m.s^{-1} (a logarithmic vertical wind profile is imposed with a roughness length of 0.2mm [8]), true wind angle β_{TW}=40 °, boat speed V_{BS}=2.6 m.s^{-1} , heel angle ϕ=20 ° and trim angle θ=0 °. This first computation yields the converged steady flow, the rig and sails' flying shape, and enables the steady state aerodynamic forces and centre of effort to be determined. This converged steady state is used as the initial condition for the computations with pitching forcing. The height z_a=6.26m of the centre of aerodynamic forces is used to define the flow characteristic quantities: apparent wind speed V_{AW}=8.81 m.s^{-1}, apparent wind angle β_{AW}=29.19 ° and sail plan chord C=6.22m defined as the distance from the head-sail

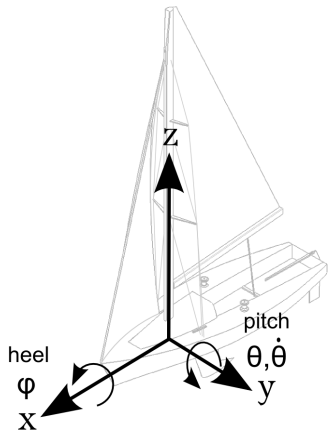

Figure 1: Coordinate, angle and motion references for the yacht. Z axis is attached to the earth vertical.

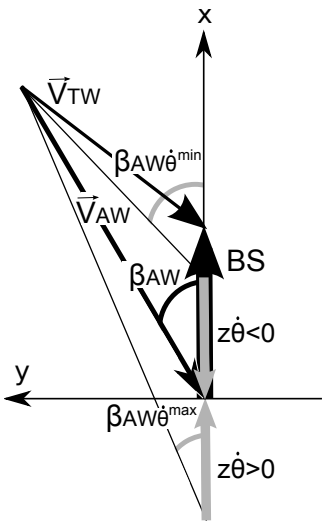

Figure 2: Dynamic effect of pitching on the wind triangle (top view). $\vec{V}$ is the wind velocity, BS is the boat speed, z is the height of the aerodynamic centre of effort, $\dot{\theta}$ is the pitching velocity, β is the apparent wind angle, subscripts TW and AW stand for True and Apparent wind

leading edge to the main sail trailing edge at z_a. Corrections of the apparent wind angle β_{AW} due to constant heel ϕ (first introduced by [19]) and trim θ are considered through the use of the effective apparent wind angle β_{eff} (see [17] for heel effect, and [12] for pitch effect):

$$\beta_{eff} = \tan^{-1}\left(\frac{\tan\beta_{AW}}{\cos\theta}\cos\phi\right) \quad (1)$$

β_{eff}=27.79 ° in the steady state.

3.2 Harmonic pitching

The unsteady computations consist of a 20s run, with forced harmonic pitching being imposed on the rig, characterised by the oscillation amplitude A and period T (equation 2), other

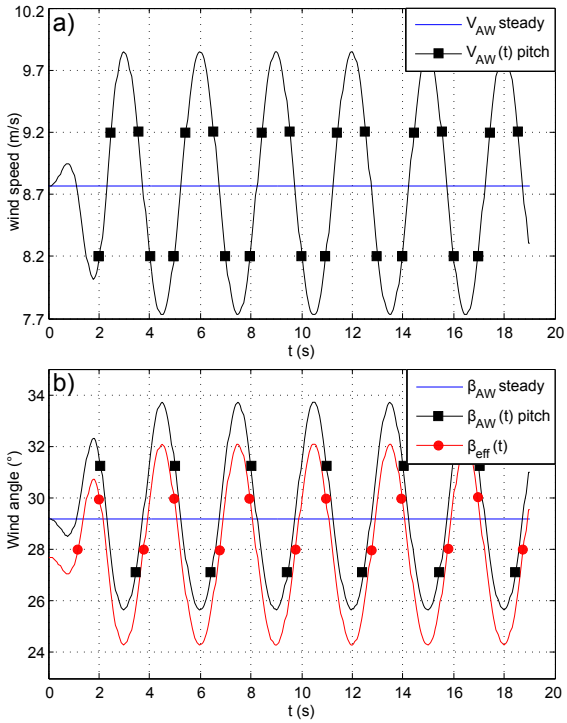

Figure 3: Time dependent apparent wind speed V_{AW} (a); apparent wind angle β_{AW} and effective wind angle β_{eff} (b) resulting from pitching oscillation at z_a with period T=3s and amplitude A=5 ° .

parameters being constant and equal to those of the reference state.

$$\theta = A\cos\left(\frac{2\pi}{T}t\right) \quad (2)$$

To avoid discontinuities in the accelerations, the beginning of motion is gradually imposed by applying a ramp which increases smoothly from 0 to 1 during the first 3s of imposed motion (see first period in Figure 3). The investigation has been made with variables in the range A=3 to 6 ° , and T=1.5 to 6s, corresponding to the typical environmental conditions encountered, as shown in the experiment of [3]. The unsteady nature of a flow is characterised by a dimensionless parameter defined by the ratio of the motion period T to the fluid advection time along the total sail plan chord C. Similarly to the closely related literature [13, 15], this parameter is called the flow reduced velocity V_r (or the inverse: the reduced frequency f_r) defined by:

$$V_r = \frac{V_{AW}T}{C} = f_r^{-1} \quad (3)$$

The case $V_r \gg 1$ ($f_r \ll 1$) corresponds to quasi-steady aerodynamic conditions. The pitching period values investigated correspond to a reduced velocity V_r from 2 to 8.5 (reduced frequency f_r from 0.12 to 0.47), which positions this numerical study in a similar dynamic range to the experiments

of [12] where V_r was from 2.3 to 56 (reduced frequency f_r from 0.02 to 0.43) corresponding to typical conditions encountered by a 48-foot yacht (14.6m). The computed cases are summarised in Table 1.

When the yacht is subjected to pitching motion, the apparent wind is periodically modified as the rotation adds a new component of apparent wind which varies with height. Following the analysis of [12], the apparent wind and pitch-induced velocity are considered at the centre of aerodynamic force height z_a. This centre of effort is actually moving due to pitch oscillation, but variations are small enough to be ignored, and the reference height computed in the steady state is used. This yields time dependent apparent wind speed and angle, given by:

$$\begin{aligned} V_{AW}(t) &= \big((V_{TW}\sin\beta_{TW})^2 \\ &\quad +(V_{TW}\cos\beta_{TW}+V_{BS}+z_a\dot{\theta}(t))^2\big)^{\frac{1}{2}} \\ \beta_{AW}(t) &= \sin^{-1}\left(\frac{V_{TW}\sin\beta_{TW}}{V_{AW}(t)}\right) \end{aligned} \tag{4}$$

And hence the time-dependent effective wind angle:

$$\beta_{eff}(t) = \tan^{-1}\left(\frac{\tan\beta_{AW}(t)}{\cos\theta(t)}\cos\phi\right) \tag{5}$$

Figure 2 illustrates the dynamic vector composition for pitching velocities $\dot{\theta}$=$\dot{\theta}_{max}$, 0 and $\dot{\theta}_{min}$, and Figure 3 shows the resulting dynamic apparent wind velocity and angle computed with equations 4 and 5. As shown in Figure 3, the apparent wind angle variations are in phase opposition with the apparent wind speed.

3.3 Heeling and driving force coefficients

Aerodynamic forces are calculated by the code at the sail plan's centre of effort. Forces are calculated in the boat frame and written in the inertial reference frame, in order to get F_x and F_y, the driving and the heeling forces. The transition matrix R_T is defined by $R_T = R_\theta R_\phi R_\alpha$ with:

$$R_\theta = \begin{bmatrix} 1 & 0 & 0 \\ 0 & \cos\theta & -\sin\theta \\ 0 & \sin\theta & \cos\theta \end{bmatrix}, R_\phi = \begin{bmatrix} \cos\phi & 0 & \sin\phi \\ 0 & 1 & 0 \\ -\sin\phi & 0 & \cos\phi \end{bmatrix}$$

$$R_\alpha = \begin{bmatrix} \cos\alpha & -\sin\alpha & 0 \\ \sin\alpha & \cos\alpha & 0 \\ 0 & 0 & 1 \end{bmatrix}$$

Driving and heeling force coefficients are obtained by the normalisation with the product of the instantaneous apparent dynamic pressure and the total sail area S:

$$C_x(t) = \frac{F_x}{0.5\rho V_{AW}^2(t)S} \tag{6}$$

$$C_y(t) = \frac{F_y}{0.5\rho V_{AW}^2(t)S} \tag{7}$$

In the steady state calculation, driving coefficient C_x=0.379 and heeling coefficient C_y=-1.226 are obtained.

4 Dynamic behaviour

Previous studies [13, 4] have shown that the dynamic behaviour of a yacht sail plan subjected to pitching clearly deviates from the quasi static approach. Particularly, the aerodynamic forces presented as a function of the instantaneous apparent wind angle show hysteresis loops as illustrated in figure 4. Different questions have been raised by this result. Is this a real hysteresis phenomenon or is this appearance in the Lissajous plot only a consequence of a simple phase shift between the signals? In the former case, can we determine the amount of energy corresponding to the hysteresis loop?

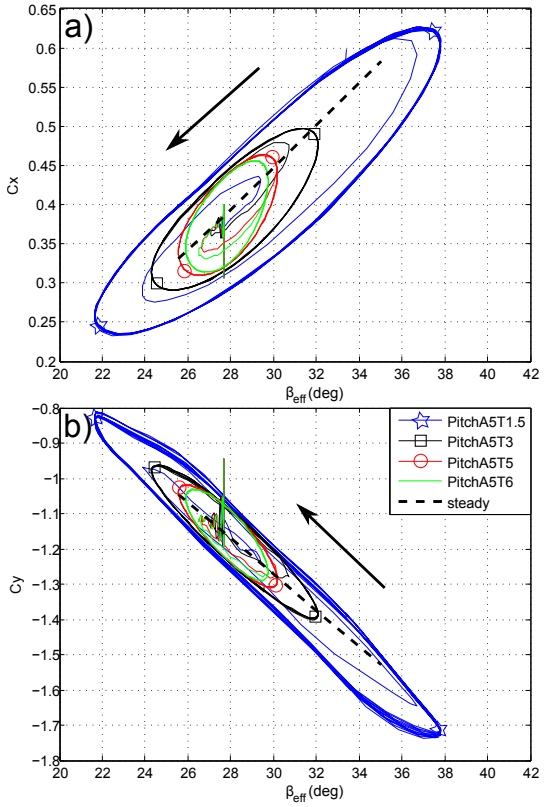

Figure 4: Driving a) and heeling b) force coefficients versus effective wind angle β_{eff}(t).

4.1 Phase shift τ

The values of the phase shift τ between aerodynamic forces and instantaneous wind angle have been determined for each pitching period and amplitude by cross-correlation (Table 1). The phase delay increases (almost linearly in the investigated range) with the flow reduced velocity (with the motion period) but is not affected by the oscillation amplitude. When forces $C_{x,y}$(t) are plotted versus the time shifted wind angle β_{eff}(t+τ), the loop area is significantly decreased but does not vanish (see Fig. 5). Even for different values of the time delay that have been tested, the loop did not collapse into a single line. The "best" time delay corresponding to the lowest area is the one computed by cross correlation. This shows

T	A	V_r	f_r	τ	$2\pi\tau$/T	W
s	deg			s	rad	
1.5	5	2.13	0.47	0.1	0.42	-3.38 e-3
3	5	4.27	0.23	0.3	0.63	-1.38 e-3
5	5	7.11	0.14	0.6	0.75	-7.18 e-4
6	5	8.53	0.12	0.75	0.79	-6.18 e-4

T	A	V_r	f_r	τ	$2\pi\tau$/T	W
s	deg			s	rad	
5	3	7.11	0.14	0.6	0.75	-2.57 e-4
5	5	7.11	0.14	0.6	0.75	-7.18 e-4
5	6	7.11	0.14	0.6	0.75	-1.04 e-3

Table 1: Reduced velocity V_r, reduced frequency f_r, phase delay τ between C_x and β_{eff} determined by cross-correlation, and non-dimensional energy W=$\int_T C_x dx$ for different pitching amplitudes A and periods T

that there is a real hysteresis phenomenon and not only a phase shift between the signals.

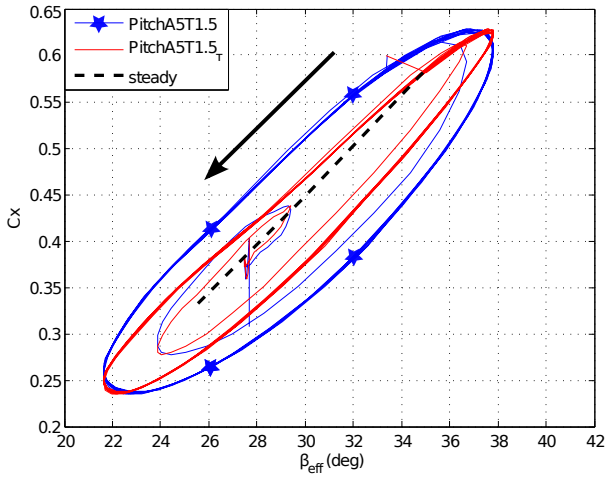

Figure 5: Driving force coefficient vs. instantaneous apparent wind angle β_{eff}(t) (blue line with markers), and vs. the time shifted instantaneous apparent wind angle β_{eff}(t+τ) (red line without marker), for a pitching period T=1.5s and amplitude A=5 °

4.2 Energy exchanged

The area contained in the hysteresis loop of Fig. 4 does not correspond to a work or energy as β_{eff} is the effective apparent wind angle and its relationship to a displacement is not straightforward. To build an energy, the displacement of the centre of effort dx along the direction of the driving force is considered, and the non-dimensional work W of the driving force during one oscillation period is defined by:

$$W = \oint C_x dx \tag{8}$$

$$dx = \frac{z_a}{C} d\theta \cos(\theta) \tag{9}$$

Figure 6 shows the driving force coefficient as a function of the non-dimensional displacement dx for different pitching periods. The area of the hysteresis loop here corresponds to a work which is the amount of energy exchanged by the system. The values obtained for each case are given in Tab. 1. The energy increases (almost linearly in the investigated range) with the pitching reduced frequency and increases (almost quadratically in the investigated range) with the pitching amplitude.

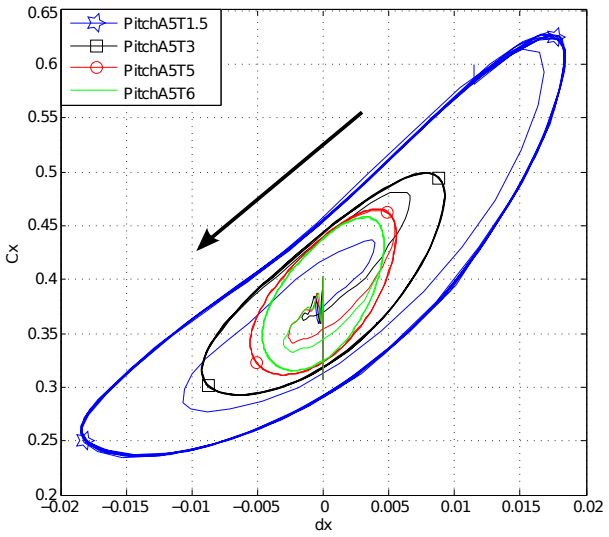

Figure 6: Driving force coefficient vs. non-dimensional displacement dx for pitching periods T=1.5, 3, 5 and 6s. The loop area represents the work exchanged W.

The aerodynamic behaviour is now clearly characterised: an hysteresis phenomenon is evidenced and the associated energy is computed. The next sections address the various influences of the yacht motion considered and of different rig trims.

5 PITCHING DECOMPOSITION

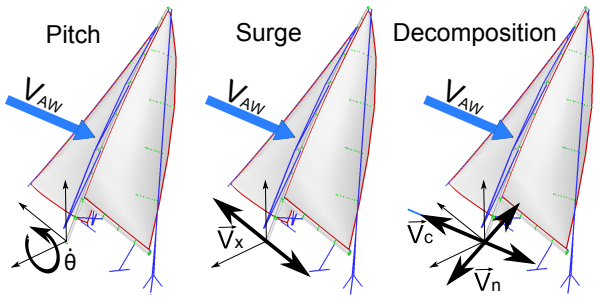

Figure 7: Different motions considered: pitching (rotation), surge (translation), surge decomposition into translations collinear to the apparent wind V_c and normal to the apparent wind V_n.

The real pitching motion is modelled here by an angular

oscillation around the y axis (Fig.7 Pitch), normal to the centreline with a rotation centre located at the mast step. Most of previous studies on the influence of pitching have considered a 2D simplified problem and thus approximated the pitching motion by a translational oscillation aligned with the yacht centreline (Fig.7 Surge). Then, the usual procedure is to decompose this motion in an oscillation parallel to the apparent wind, resulting in an oscillation of apparent wind speed, and an oscillation orthogonal to the apparent wind, resulting mainly in an oscillation of the apparent wind angle [15] (Fig.7 decomposition). Here, we want to test these two hypotheses by comparing the results of the dynamic simulation with ARAVANTI obtained with different imposed motions, and investigate the effect on the specific dynamic features highlighted above. Motions are based on the standard pitching motion with amplitude A=5 ° and period T=5s (A5T5).

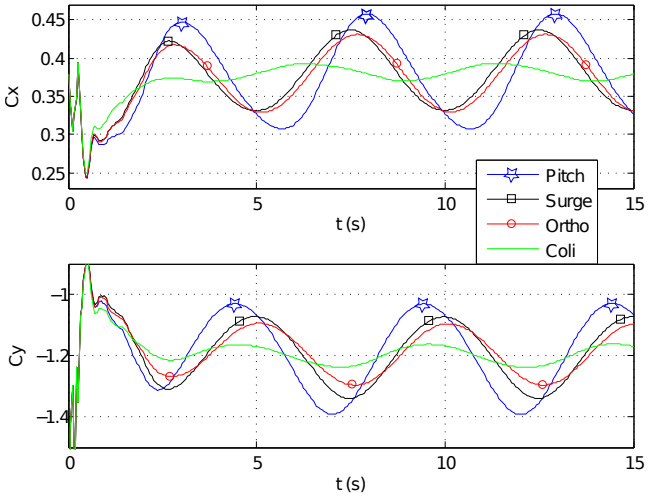

Figure 8: Time series of the driving and heeling force coefficients for FSI simulations of the various motions considered: pitching, surge, translations collinear and perpendicular to the apparent wind (see Fig.10), corresponding to a pitching amplitude A=5 ° and period T=5s.

5.1 Surge

The first step is to compare the results with a real pitching motion (rotation) to the results with a translational surge motion with the amplitude of motion at the centre of effort height while pitching. As shown on Fig 8 the oscillation of aerodynamic forces is decreased by 25% and phase shifted (around T/10) when the pitching is reduced to a surge motion. This result gives the order of the error introduced by considering a surge motion instead of the pitching motion.
Concerning the dynamic behaviour, it is interesting to notice that the case of surge does not show the same hysteresis phenomenon. Indeed, the aerodynamic behaviour in the case of surge is much closer to the quasi-steady theory than in the pitching case, as clearly shown on Fig 9. The loop of $C_{x,y}(\beta_{eff})$ collapses and is superposed to the quasi-steady line.

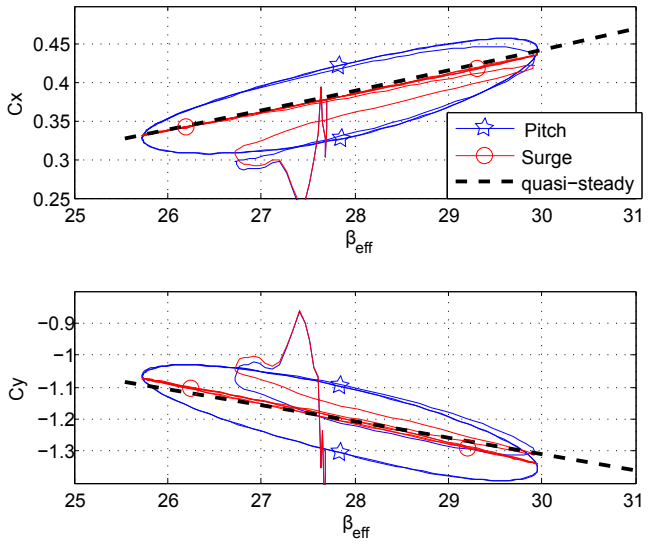

Figure 9: Driving and heeling force coefficients versus apparent wind angle for pitch and surge motion. The motion period and amplitude at the centre of effort are identical and correspond to a pitching amplitude A=5 ° and period T=5s.

5.2 Simple translations decomposition

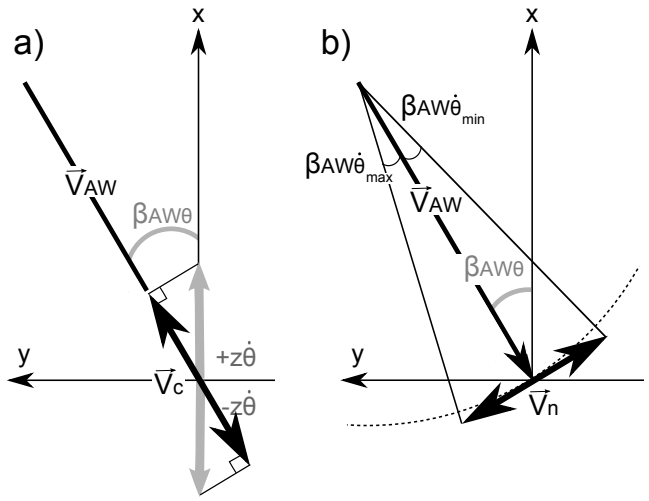

Figure 10: Wind triangle representation for the surge decomposition into 2 translations a) V_c collinear to V_{AW} and b) V_n normal to V_{AW}.

The second step is to analyse separately the effects of translational oscillations parallel V_c (Fig 10.a) and orthogonal V_n (Fig 10.b) to the apparent wind direction. It is observed on Fig. 8 that the major contribution to the force oscillation is due to the orthogonal oscillation component, which is associated to the oscillation of apparent wind angle. When the variations due to both components of motion are added (not shown on Fig. 8 for clarity), the result is very similar to what is obtained with the surge motion (maximum of cross-correlation= 0.998), which justifies the linear superposition principle of

this approach. The effect of parallel oscillation —variation of AWS(t)— is small, but with an important phase shift (about T/3).

Moreover, one can notice that the oscillation of forces is not symmetric — the duration of increasing and decreasing phases are different— for pitching, surge and parallel oscillation, but it is symmetric for the orthogonal oscillation. This can be explained in the following way. The orthogonal oscillation is associated to an oscillation of AWA(t), and the effect of angle of attack in a narrow range is almost linear on the aerodynamic lift. Contrarily, the parallel oscillation is associated with an oscillation of AWS(t), and the effect of wind speed is quadratic on aerodynamic forces.

6 INFLUENCE OF RIG ADJUSTMENTS

In this section, the analysis of the effects of various dock tunes and backstay loads on the dynamic behaviour and the energy exchanged is presented.

6.1 Influence of dock tune

The influence of various dock tunes on the sail plan dynamic behaviour is investigated. The same pitching motion (A=5 ° and T=5s) is simulated with three realistic dock tunes used while racing in different wind conditions. Dock tunes are defined as the number of screw turns applied to the shrouds' turn-buckles. Tune$_2$ is the reference dock tune used for the considered sailing conditions. The three dock tunes are described bellow:

- tune$_1$: -3 turns on V1 shrouds used in light wind
- tune$_2$: reference dock tune
- tune$_3$: +3 turns on V1 shrouds used in medium wind

This three dock tunes not only modify the rigidity of the full rigging but have a significant influence on the camber and maximum camber height of the mast. The sails' shape and more precisely their camber and twist are modified by the dock tune. Before the pitching simulation, the main sail and jib are trimmed in order to ensure that the chord at the centre of effort height has the same angle of attack for the different tunes. The centre of effort height z_a is identical for the three dock tunes.

Figure 11 illustrates the driving force coefficient evolution versus the non-dimensional displacement dx. The loops look similar, however, the exchanged energy computed as described in section 4 shows variations. Table 2 presents the relative evolution of the mean driving force and exchanged energy compared to the reference dock tune tune$_2$.

The effect of various dock tunes on the mean driving force and energy inside the hysteresis loop is not very strong, but trends can nevertheless be noticed. For the same wind velocity and pitching amplitude and period, the energy associated to the driving force hysteresis is increased by 3% for the less tight dock-tune (tune$_1$) and reduced by 4% for the tightest dock-tune (tune$_3$), compared to the reference. The effect on mean driving force is only of order 1% in the same direction.

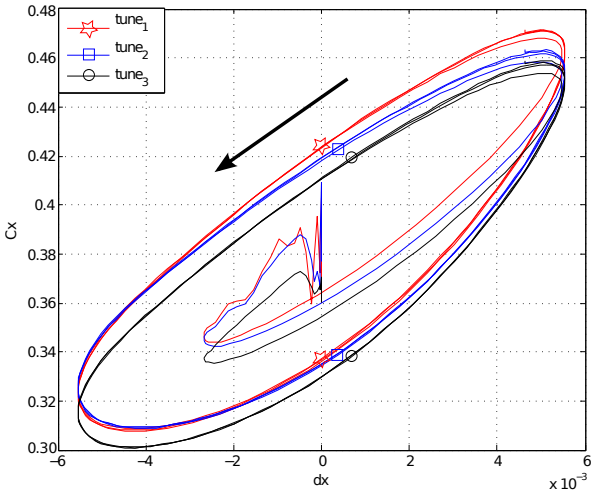

Figure 11: Driving force coefficient vs. non-dimensional displacement dx for different dock tunes, for a pitching amplitude A=5 ° and period T=5s. The loop area represents the work exchanged.

dock tune	$\frac{W}{W_{tune_2}}$	$\frac{\bar{C_x}}{\bar{C}_{x\,tune_2}}$	$\frac{\bar{C_y}}{\bar{C}_{y\,tune_2}}$
tune$_1$	1.029	1.007	1.006
tune$_2$	1	1	1
tune$_3$	0.960	0.983	0.987

Table 2: Non-dimensional work W=$\int_T C_x dx$ associated to hysteresis loop, mean driving force coefficient $\bar{C_x}$ and mean heeling force coefficient $\bar{C_y}$ for different dock tunes, relative to reference case (tune$_2$), for a pitching amplitude A=5 ° and period T=5s.

6.2 Influence of the backstay load

The influence of a variation of the backstay tension on the dynamic behaviour is investigated. The same pitching motion (A=5 ° and T=5s) is simulated with four values of backstay load: 1000N, 1500N, 2000N and 2500N. The case 2000N is the reference backstay load used for the previous simulations. The sail trims are identical for the four backstay loads.

Preliminary steady simulations with the four loads have shown the ability of ARAVANTI model to simulate the effect of the backstay: the main twist increases, the main camber decreases and moves backward when the backstay load increases.

Figure 12 illustrates the driving force coefficient evolution versus the non-dimensional displacement dx. As expected, the mean driving and heeling forces are greatly affected by the backstay load, which changes the main sail camber and twist (see Tab. 3).

The backstay load also has a great influence on the energy contained in the hysteresis loop (see Tab. 3). The computed work decreases when load in the backstay is increased. This interesting observation could be due to the great importance of the rig flexibility under pitching. The reduction of energy

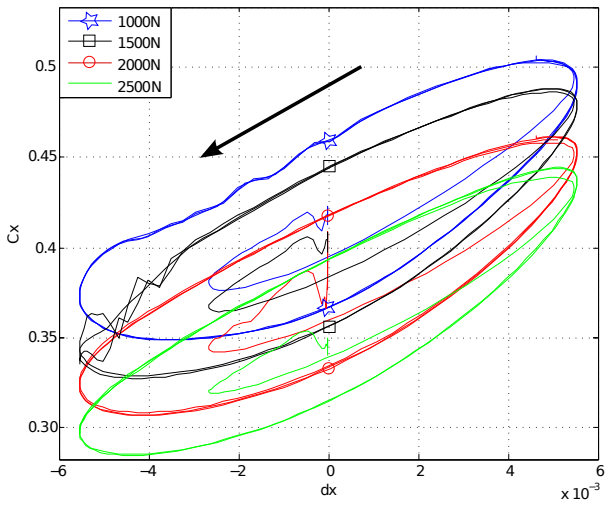

Figure 12: Driving force coefficient vs. non-dimensional displacement dx for different backstay loads, for a pitching amplitude A=5 ° and period T=5s. The loop area represent the work exchanged W.

Load	$\frac{W}{W_{2000N}}$	$\frac{\bar{C_x}}{\bar{C}_{x\,2000N}}$	$\frac{\bar{C_y}}{\bar{C}_{y\,2000N}}$
1000N	1.100	1.087	1.119
1500N	0.994	1.038	1.052
2000N	1	1	1
2500N	0.938	0.932	0.931

Table 3: Non-dimensional work W=$\int_T C_x dx$, mean driving force coefficient $\bar{C_x}$ and mean heeling coefficient $\bar{C_y}$ for different backstay loads, relative to reference case (2000N), for a pitching amplitude A=5 ° and period T=5s.

exchanged with the increase of load in the backstay seems to be due to higher longitudinal stresses on the rigging. With more stresses, the rig is getting closer to a rigid structure and comparison between FSI and rigid simulation [4] has shown that the hysteresis phenomenon is significantly lower in the rigid case.

7 CONCLUSIONS

The unsteady fluid structure interaction of the sails and rig of a 28-foot (8m) yacht under harmonic pitching has been investigated in order to highlight the contributions of the rig adjustments and the consideration of a realistic pitching motion in the dynamic behaviour of a sail plan. The ARAVANTI model is based on an implicit unsteady coupling between a vortex lattice fluid model and a finite element structure model, and has been previously validated with full scale experiments in upwind real conditions [3]. Previous studies [13, 4] have shown that the aerodynamic coefficients plotted against the instantaneous apparent wind angle exhibit an hysteresis loop. These results confirm that the dynamic behaviour of a sail plan subject to yacht motion deviates from the quasi-steady theory. Oscillations of the aerodynamic forces exhibit phase shifts and hysteresis which increase with the motion reduced frequency and amplitude.

In this article, it is shown that the loop area is not only due to the phase shift. After shifting by the phase delay τ, the hysteresis loop of $C_{x,y} = f(\beta_{eff}(t+\tau))$ does not collapse into a single line.

The energy contained in the hysteresis loop is determined by integration of the driving force along the back and forth motion due to pitching at the centre of effort height. The resulting work is shown to increase with the pitching frequency and amplitude. Further work is needed to better understand the energy transfer in the system, and to confirm the evolution of phase shift and amount of energy on a larger motion parameters' range.

Pure harmonic surge motion is compared to pitching motion in order to highlight the importance of a realistic 3D motion. Oscillations of the aerodynamic coefficients decrease by 25% in the case of surge motion compared to the pitching motion case. Moreover, in the case of the surge motion, the hysteresis phenomenon is almost cancelled, so that the dynamic behaviour is similar to the quasi-steady theory. When the surge motion is decomposed into two components, perpendicular to and along the apparent wind direction, it is shown that the major contribution to force oscillation is due to the orthogonal oscillation component, which is associated to the oscillation of apparent wind angle.

Finally, a pitching motion of the structure with various shrouds' dock tunes and backstay tension loads is simulated in order to study the influence of the rigging stresses on the dynamic behaviour. Both mean driving force and work inside the hysteresis loop are decreased when the stresses in the rig are increased.

Acknowledgements

The authors are grateful to K-Epsilon company for continuous collaboration. This work was supported by the French Naval Academy.

References

[1] B. Augier, P. Bot, F. Hauville, and M. Durand. Experimental validation of unsteady models for Wind / Sails / Rigging Fluid structure interaction. *International Conference on Innovation in High Performance Sailing Yachts, Lorient, France*, 2010.

[2] B. Augier, P. Bot, F. Hauville, and M. Durand. Experimental full scale study on yacht sails and rig under unsteady sailing conditions and comparison to fluid structure interaction unsteady models. *The 20th Chesapeake Sailing Yacht Symposium, Annapolis USA*, 2011.

[3] B. Augier, P. Bot, F. Hauville, and M. Durand. Experimental validation of unsteady models for fluid structure interaction: Application to yacht sails and rigs. *Journal of Wind Engineering and Industrial Aerodynamics*, 101(0):53 – 66, 2012.

[4] B. Augier, P. Bot, F. Hauville, and M. Durand. Dynamic Behaviour of a Flexible Yacht Sail Plan. *Journal of Ocean Engineering*, 66:32–43, 2013.

[5] V. Chapin and P. Heppel. Performance optimization of interacting sails through fluid structure coupling. *2nd International Conference on Innovation in High Performance Sailing Yachts, Lorient, France*, 2010.

[6] T. Charvet, F. Hauville, and S. Huberson. Numerical simulation of the flow over sails in real sailing conditions. *Journal of Wind Engineering and Industrial Aerodynamics*, 63(1-3):111 – 129, 1996.

[7] A. D. Fitt and T. R. B. Lattimer. On the unsteady motion of two-dimentional sails. *J. Appl. Maths*, 65:147–171, 2000.

[8] R. G. J. Flay. A twisted flow wind tunnel for testing yacht sails. *Journal of Wind Engineering and Industrial Aerodynamics*, 63(13):171 – 182, 1996. Special issue on sail aerodynamics.

[9] F. Fossati. *Aero-Hydrodynamics and the Performance of Sailing Yachts: The Science Behind Sailing Yachts and Their Design*. Adlard Coles Nautical, 2010.

[10] F. Fossati and S. Muggiasca. Sails Aerodynamic Behavior in dynamic condition. *The 19th Chesapeake Sailing Yacht Symposium, Annapolis, USA*, 2009.

[11] F. Fossati and S. Muggiasca. Numerical modelling of sail aerodynamic behavior in dynamic conditions. *2nd International Conference on Innovation in High Performance Sailing Yachts, Lorient, France*, 2010.

[12] F. Fossati and S. Muggiasca. Experimental investigation of sail aerodynamic behavior in dynamic conditions. *Journal of sailboat technology*, (03), 2011.

[13] F. Fossati and S. Muggiasca. An experimental investigation of unsteady sail aerodynamics including sail flexibility. *4th High Performance Yacht Design Conference Auckland, New Zeeland*, 2012.

[14] R. Garrett. *The symmetry of sailing: the physics of sailing for yachtsmen*. Sheridan House, Inc., 1996.

[15] F. Gerhardt, Richard Go Jo Flay, and Patrick Jo Richards. Unsteady aerodynamics of two interacting yacht sails in two-dimensional potential flow. *Journal of Fluid Mechanics*, 668(1):551–581, 2011.

[16] F. Hauville, M. Durand, and Y. Roux. Aero elastic model applied to the deformation of a rig. *European Journal of Environmental and Civil Engineering*, 12(5):549 – 560, 2008.

[17] P.S. Jackson. An improved upwind sail model for vpps. *The 15th Chesapeake Sailing Yacht Symposium, Annapolis, USA*, 2001.

[18] J.A. Keuning, K.J. Vermeulen, and E.J. de Ridder. A generic mathematical model for the manoeuvring and tacking of a sailing yacht. *The 17th Chesapeake Sailing Yacht Symposium, Annapolis, USA*, pages 143–163, 2005.

[19] C.A. Marchaj. *Sail performance: techniques to maximize sail power*. International Marine/Ragged Mountain Press, 1996.

[20] Y. Masuyama and T. Fukasawa. Full scale measurement of sail force and the validation of numerical calculation method. *The 13th Chesapeake Sailing Yacht Symposium, Annapolis, USA*, 1997.

[21] Y. Masuyama, Y. Tahara, T. Fukasawa, and N. Maeda. Dynamic performance of sailing cruiser by a full scale sea reality. *The 11th Chesapeake Sailing Yacht Symposium, Annapolis, USA*, 1993.

[22] H. Renzsh and K. Graf. Fluid Structure Interaction simulation of spinnakers - Getting closer to reality. *2nd International Conference on Innovation in High Performance Sailing Yachts, Lorient, France*, 2010.

[23] T. Richardt, S. Harries, and K. Hochkirch. Maneuvering simulations for ships and sailing yachts using friendship-equilibrium as an open modular workbench. *International Euro-Conference on Computer Applications and Information Technology in the Maritime Industries*, 2005.

[24] Y. Roux, M. Durand, A. Leroyer, P. Queutey, M. Visonneau, J. Raymond, J.M. Finot, F. Hauville, and A. Purwanto. Strongly coupled VPP and CFD RANSE code for sailing yacht performance prediction. *3rd High Performance Yacht Design Conference Auckland, New Zeeland*, 2008.

[25] Y. Roux, S. Huberson, F. Hauville, J.P. Boin, M. Guilbaud, and M. Ba. Yacht performance prediction: Towards a numerical vpp. *High Performance Yacht Design Conference*, 2002.

[26] H. Schoop and N. Bessert. Instationary aeroelastic computation of yacht sails. *International Journal for Numerical Methods in Engineering*, 52(8):787–803, 2001.

AUTHORS BIOGRAPHY

Benoit Augier holds the current position of post doc fellow in Department of Structural Engineering at UCSD, San Diego, USA. He obtained his Ph.D. at the Naval Academy Research Institute, Brest, France in 2012. His research interests include Fluid Structure Interaction, Dynamic behaviour of a soft membrane, Full Scale Experiment and CFD Simulations.

Frédéric Hauville holds the current position of Associate Professor at Naval academy Research Institute-IRENav. He is co-responsible of the Voil'Enav project which concerns activities in the field of fluid dynamics applied to sailing yachts. His current research interests includes, both by

numerical and experimental approaches, problems of fluid structure interaction applied to the deformation of flexible surfaces and the hydrodynamic study of the forced moving foils applied to propulsion and marine current turbines. His previous experience includes a PhD in fluid dynamic in 1996.

Patrick Bot holds the current position of associate professor at the Naval Academy Research Institute in fluid mechanics and energy engineering. His research interests include yacht dynamics, sail aerodynamics and fluid structure interaction. His previous experience includes hydrodynamic instabilities and transition to turbulence.

Mathieu Durand holds the current position of R&D director at K-Epsilon company. He is responsible for FSI developments and sails simulations. His previous experience includes a PhD in fluid dynamic in 2012, but also sailing experience as match-racing skippers (#40 in world ranking in 2011).

Julien Deparday is a Ph.D. student at the Naval Academy Research Institute. He is studying the Fluid Structure Interaction on soft surfaces applied to sails. He is in charge of the experimental work.